

Theory and Design of Multirate Sensor Arrays

Omid S. Jahromi, *Member, IEEE*, and Parham Aarabi, *Member, IEEE*

Artificial Perception Laboratory

Edward S. Rogers Sr. Department of Electrical and Computer Engineering

University of Toronto

Toronto, Ontario, Canada M5S 3G4

Phone: (416) 946-7893 Fax: (416) 978-4425

Email: omidj@control.toronto.edu, parham@ecf.toronto.edu

EDICS: 2-FILB , 2-MWAV,

Corresponding author: Omid Jahromi

Abstract

This paper studies the basic design challenges associated with multirate sensor arrays. A multirate sensor array is a sensor array in which each sensor node communicates a low-resolution measurement to a central processing unit. The objective is to design the individual sensor nodes and the central processing unit such that, at the end, a unified high-resolution measurement is reconstructed

A multirate sensor array can be modelled as an analysis filter bank in discrete-time. Using this model, the design problem is reduced to solving the following two problem: (a) How to design the sensor nodes such that the time-delay of arrival (TDOA) between the sensors can be estimated using the low-rate data sent by them? (b) How to design a synthesis filter bank to fuse the low-rate data sent by the sensor nodes given the TDOA?

We show that it is possible to estimate the TDOA between the sensors if the analysis filters incorporated in the array satisfy specific phase-response requirements. We then provide practical sample designs which satisfy these requirements. We prove, however, that a fixed synthesis filter bank can not reconstruct the desired high-resolution measurement for all TDOA values. As a result, we suggest a fusion system which uses different sets of synthesis filters for even and odd TDOAs. Finally, we use the \mathcal{H}_∞ optimality theory to design optimal synthesis filters.

I. INTRODUCTION

In recent years there has been an emergence of several new distributed sensing concepts. In particular, distributed sensor arrays incorporating a large of number of tiny, inexpensive sensors interconnected via wireless data networks have attracted considerable attention [1], [2]. Such networked sensor arrays can, in principle, provide enhanced spatio-temporal sensing coverage in ways that are either prohibitively expensive or simply impossible using conventional sensing assets. However, small and inexpensive sensing nodes are inherently constrained in computation and communication capabilities. Furthermore, price, power consumption, and network data rate limitations prohibit individual sensor nodes from acquiring and/or transmitting high-resolution measurement data. Effective application of such sensors, thus, requires multirate signal processing techniques whereby a unified high-resolution measurement is produced from the low-resolution data communicated by individual sensor nodes. A simple two-node multirate sensor system is described in the following example.

Example 1: Consider the setup in Fig. 1(a). Here, $x(t)$ denotes the signal arriving at the reference sensor node. This signal is the object of measurement. Assuming that attenuation is negligible and the environment is non-dispersive, the signal received by the second sensor is $x(t - \Delta)$ where Δ represents the unknown

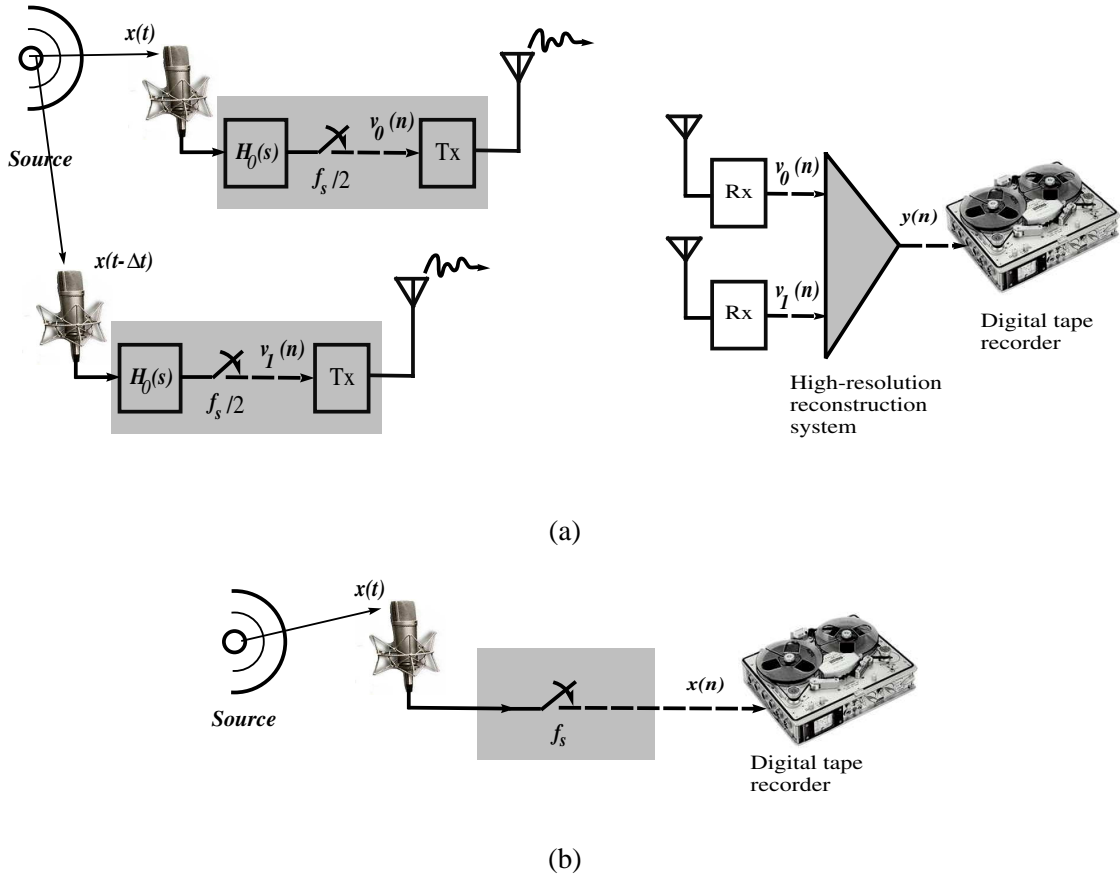


Fig. 1. (a) A two-node multirate sensor array system. Each sensor node samples and communicates data at only half of the Nyquist rate required to discretize the signal $x(t)$ faithfully. The objective is to design the sensor nodes and the reconstruction system at the receiving end such that the signal $y(n)$ reconstructed at the receiver is a replica of the direct high-sampling-rate measurement $x(n)$ shown in (b).

time-delay of arrival (TDOA) in seconds. Each sensor node includes an internal filter $H_i(s)$ chosen by the system designer, a sampling device and a digital transmitter. The discrete-time signals $v_i(n)$, $i = 0, 1$, produced after sampling are communicated via a digital communication network to the central station for processing¹.

Assume that the effective bandwidth of $x(t)$ is W Hz. Thus, the minimum (Nyquist) sampling frequency needed for aliasing-free discretization of $x(t)$ is $f_s \triangleq 2W$. Assume, however, that the sampling devices in the sensor nodes work at $f_s/2$ due to transmission rate limitations imposed by the communication network.

¹For simplicity, the quantization effects inherent in the digital transmission are ignored. Also, the measurements $v_i(n)$ are assumed to be decoded at the receiver in such a way that their relative synchronization is preserved. If there is a time-delay of transmission, its value should be considered while calculating the TDOA in the receiver.

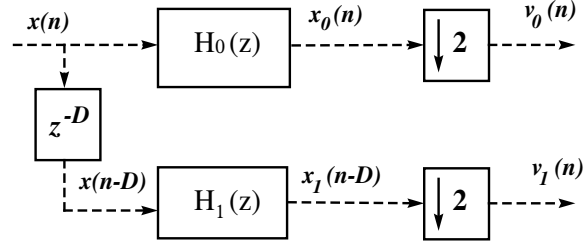


Fig. 2. Discrete-time filter bank model of the multirate sensor array shown in Fig. 1(a).

The central processing unit receives both $v_0(n)$ and $v_1(n)$ at sampling rate $f_s/2$. It then uses a reconstruction system to fuse $v_i(n)$ and generate a synthetic signal $y(n)$ with sampling rate f_s .

The design objective is to make the synthesized signal $y(n)$ a (possibly delayed and scaled) replica of $x(n)$, where $x(n)$ denotes the continuous reference signal $x(t)$ sampled at the Nyquist rate (Fig. 1(b)). In other words, the multirate sensor array should be designed such that $y(n) = cx(n - T_d)$ where $c \neq 0$ and $T_d \in \mathbb{N}$ are constants. \diamond

If we assume that TDOA is an integer multiple of the Nyquist sampling period, that is, if $\Delta \triangleq D/f_s$, $D \in \mathbb{Z}$, then the sensor node model shown in Fig. 1(a) can be discretized, leading to filter bank model shown in Fig. 2. This model clearly shows the relation between the synthesized measurement $y(n)$ and the desired (but unavailable) high-sampling-rate measurement $x(n)$. When Δ is not an integer multiple of the Nyquist sampling period $1/f_s$, the transfer function z^{-D} in Fig. 2 has no formal meaning. However, since $x(t)$ is assumed to be bandlimited to $W = f_s/2$ Hz, it can be interpreted in light of the following generalized interpolation formula [3, Sec 3.5], [4, Sec 4.2.2]:

$$Y(z) = z^{-D}X(z) \Leftrightarrow y(n) = \sum_{k=-\infty}^{\infty} x(k) \frac{\sin(\pi(n - D - k))}{\pi(n - D - k)}$$

Based on the discrete-time model shown in Fig. 2, designing a multirate sensor array requires solving the following fundamental problems:

Problem 1—Sensor Node Design: Design the equivalent filters $H_i(z)$ such that

- (a) the TDOA D can be estimated in the central processing unit from the low-rate measurements $v_i(n)$ sent by the sensors.
- (b) the analysis filter bank shown in Fig. 2 is *perfect reconstruction* for all TDOA values. That is, there exist a causal and stable synthesis filter bank with input $v_i(n)$ and output $y(n)$ such that, for all D , $y(n) = cx(n - T_d)$ where $c \neq 0$ and $T_d \in \mathbb{N}$ are constants.

Problem 2—Reconstruction System Design: Given the low-rate measurements $v_i(n)$ received by the central processing unit,

- (a) estimate the TDOA D .
- (b) find a causal and stable synthesis filter bank to reconstruct $x(n)$ from $v_i(n)$.

In recent years, extensive research has been conducted on filter banks and multirate signal processing [5], [6], [7]. However, TDOA estimation from low-rate signals and reconstruction problems involving TDOA have not been considered. In this paper, we focus on solving Problems 1 and 2 for the basic case where the array consists of only two sensors². In our experiments and simulation examples, we will use microphones as sensing devices and sound as the object of measurement. However, the paper’s theoretical results are quite general and applicable to many other sensing situations as well. Some of the results in this paper were presented in our conference paper [8].

The material in the rest of this paper are organized as follows: In Section II, we provide a brief background on TDOA estimation using the generalized cross-correlation technique. Then, we derive conditions on the analysis filters used in the sensor array so that this technique can be applied to low-rate measurements as well. We introduce sample designs and provide experiments to illustrate that these designs produce reliable TDOA estimates in practice. Section III is devoted to the technical problems that arise because of TDOA when one tries to simulate a high-resolution measurement from low-rate sensor data. In Section IV we use \mathcal{H}_∞ optimality criterion and design synthesis filters which guarantee precision fusion under all TDOA circumstances. The paper concludes by summarizing the results and discussing some open issues in Section VI.

Notation: Vectors are denoted by capital or boldface lower-case letters. Boldface capital letters are reserved for matrices. We use the notation $\stackrel{\mathcal{F}}{\rightleftharpoons}$ when two quantities are related by the discrete-time Fourier transform. The expected value of a random variable x is denoted by $E\{x\}$. The symbol \triangleq is used to indicate that two quantities are equal by definition. The Hilbert space of square-summable discrete-time signals is denoted by ℓ_2 . In diagrams, solid lines are used to represent analog signals whereas dotted lines denote discrete-time signals. The end of an example is marked using the symbol \diamond .

²Generalizing the results to N -node multirate arrays is left for future research.

II. TIME-DELAY ESTIMATION IN MULTIRATE SENSOR ARRAYS

A. Introduction

TDOA estimation arises in a variety of fields, including sound localization and processing using microphone arrays [9], [10], [11]. As a result, various algorithms have been developed for the estimation of TDOAs between two signals. The general discrete-time model can be stated as follows:

$$u_0(n) = x(n) + s_0(n) \quad (1)$$

$$u_1(n) = x(n - D) + s_1(n) \quad (2)$$

where $u_0(n)$ and $u_1(n)$ are the two signals at the observation points (i.e. sensors), $x(n)$ is the signal of interest that is referenced (zero time-delay) according to the first sensor and will have a delay of D by the time it arrives at the second sensor, and $s_0(n)$ and $s_1(n)$ are the (possibly dependent) noises of the first and second sensors, respectively.

The goal of TDOA estimation is to estimate D given a segment of data obtained from each sensor, without any prior knowledge regarding the source signal $x(n)$ or the noises. This problem has been extensively explored in the past, and depending on the application at hand, different approaches have been proposed [9], [11]. For a basic introduction to the TDOA estimation problem as well as a generalization of the widely used cross correlation based class of algorithms, the reader is referred to [11], [12]. Further analysis of TDOA estimation for microphone arrays is performed in [9], [13].

The most commonly used TDOA estimation algorithm is the cross correlation based technique, which has been widely used for a long time and generalized in [11]. The generalized approach is defined below:

$$\hat{D} = \arg \max_D \int_{\omega} Q(e^{j\omega}) U_0(e^{j\omega}) U_1^*(e^{j\omega}) e^{-j\omega D} d\omega \quad (3)$$

where $U_0(e^{j\omega})$ and $U_1(e^{j\omega})$ are the discrete-time Fourier transforms of the signals $u_0(n)$ and $u_1(n)$ respectively and $Q(e^{j\omega})$ is a cross-correlation weighting function.

While various weighting functions have been proposed in the past [11], [9], for microphone array based TDOA estimation, the PHASE Transform (PHAT) or whitening filter weights are commonly used due to the robustness of the resulting technique to reverberations [9], [14]. Using the PHAT weighting function:

$$Q(e^{j\omega}) = \frac{1}{|U_0(e^{j\omega})U_1(e^{j\omega})|} \quad (4)$$

the following PHAT form of the cross correlation is obtained:

$$\hat{D} = \arg \max_D \int_{\omega} \cos(\omega D - (\angle U_0(e^{j\omega}) - \angle U_1(e^{j\omega}))) d\omega \quad (5)$$

The PHAT technique will be used for TDOA estimation in this paper. While there are many alternatives to this approach, PHAT was chosen because of its widespread use for microphone array based TDOA estimation as well as its robustness to reverberation artifacts.

B. PHAT for low-rate signals

In this section we show that under certain conditions, the unknown time delay D can be estimated by examining the phase of the cross spectral density (CSD) $P_{v_0v_1}(e^{j\omega})$ of the low-rate signals $v_0(n)$ and $v_1(n)$. Our key result is stated in the theorem below.

Theorem 1: Assume that the TDOA D is an integer and let $W(e^{j\omega}) \triangleq H_0(e^{j\omega})H_1^*(e^{j\omega})$ where $H_0(z)$ and $H_1(z)$ are the analysis filters shown in Fig. 2. If $\angle W(e^{j\frac{\omega}{2}}) = \angle W(e^{j(\pi - \frac{\omega}{2})})$, then

$$\angle P_{v_0v_1}(e^{j\omega}) = \begin{cases} -D\frac{\omega}{2} + \angle W(e^{j\frac{\omega}{2}}) & D \text{ even} \\ -D\frac{\omega}{2} + \angle W(e^{j\frac{\omega}{2}}) + \lambda(\omega)\pi & D \text{ odd} \end{cases}$$

where $\lambda(\cdot)$ is a binary-valued function of ω assuming the values 0 and 1 only.

Proof: See Appendix I. ■

The above theorem shows that, under suitable conditions on the phase of the analysis filters, the time delay D can be recovered by examining the phase of the cross spectral density of the low-rate measurements $v_0(n)$ and $v_1(n)$. In practice, one has to start with an estimate $\hat{P}_{v_0v_1}(e^{j\omega})$ of the cross spectral density of the low-rate measurements. The estimate $\hat{P}_{v_0v_1}(e^{j\omega})$ can be obtained using any of the standard spectral estimation methods [15], [16]. Then, $\angle \hat{P}_{v_0v_1}(e^{j\omega})$ is used to calculate an estimate \hat{D} of the actual time delay D by maximizing the PHAT integral

$$\hat{D} = \arg \max_D \int_{\omega} \cos\left(-D\frac{\omega}{2} - (\angle \hat{P}_{v_0v_1}(e^{j\omega}) - \angle W(e^{j\frac{\omega}{2}}))\right) d\omega. \quad (6)$$

In principle, PHAT is a nonlinear regression method which fits the linear model $-D\frac{\omega}{2}$ to the data represented by $\angle \hat{P}_{v_0v_1}(e^{j\omega}) - \angle W(e^{j\frac{\omega}{2}})$. If D is even and the available estimate $\hat{P}_{v_0v_1}(e^{j\omega})$ is accurate, then Theorem 1 shows that $\angle \hat{P}_{v_0v_1}(e^{j\omega}) - \angle W(e^{j\frac{\omega}{2}})$ will be close to the linear function $-D\frac{\omega}{2}$. In this

case, the PHAT integral (6) produces accurate TDOA estimates. When D is odd, Theorem 1 indicates that $\angle \hat{P}_{v_0 v_1}(e^{j\omega}) - \angle W(e^{j\omega})$ will be close to $-D\frac{\omega}{2} + \lambda(\omega)\pi$. The binary-valued function

$$\lambda(\omega) \triangleq \begin{cases} 0 & \text{if } P_{xx}(e^{j\frac{\omega}{2}}) \left| W(e^{j\frac{\omega}{2}}) \right| > P_{xx}(e^{j\frac{\omega-2\pi}{2}}) \left| W(e^{j\frac{\omega-2\pi}{2}}) \right| \\ 1 & \text{if } P_{xx}(e^{j\frac{\omega}{2}}) \left| W(e^{j\frac{\omega}{2}}) \right| < P_{xx}(e^{j\frac{\omega-2\pi}{2}}) \left| W(e^{j\frac{\omega-2\pi}{2}}) \right| \end{cases} \quad (7)$$

is representative of the sign ambiguity which occurs in the determining the phase of $P_{v_0 v_1}(e^{j\omega})$. As can be seen from the expression above, $\lambda(\omega)$ depends on the input signal statistics through $P_{xx}(e^{j\omega})$.

In principle, it is possible to estimate $P_{xx}(e^{j\omega})$ from $v_0(n)$ and $v_1(n)$ using the technique described in [17] and then estimate $\lambda(\omega)$ from (7). However, we do not follow this possibility here due to its very high computational burden. Instead, we choose to ignore the term $\lambda(\omega)\pi$ while calculating the PHAT integral. Our rationale is that for most sensor array applications (e.g., microphone arrays), the low-frequency half of the spectrum hugely dominates the high frequency half in terms of energy. As a result, $\lambda(\omega)$ will be equal to zero much more frequently than 1. This makes the overall contribution of the term $\lambda(\omega)\pi$ to the PHAT integral (6) negligible. We will demonstrate the general validity of this assumption in Section II-D where we present actual TDOA estimation experiments. There, we will provide cases where this assumption fails to hold as well.

Remark 1: The results of Theorem 1 remain valid even when independent noise components $s_0(n)$ and $s_1(n)$ are added to the input signals $x(n)$ and $x(n - D)$, respectively. However, if the noise sources $s_0(n)$ and $s_1(n)$ are correlated, an extra term (which depends on the cross-correlation between the two noise signals) will be added to the right hand side of (22). This will introduce additional terms in the phase of $P_{v_0 v_1}(e^{j\omega})$ and, hence, bias in the estimation of D . Our experiments with microphone arrays showed that nominal room noise (air conditioning systems, etc. resulting in 20dB SNR) had no noticeable effect on the accuracy of TDOA estimates (See the experiments in Section II-D).

Remark 2: The TDOA estimator \hat{D} given by (6) is robust and does not collapse if the actual TDOA is not an integer multiple of the sampling interval. In fact, Theorem 1 is valid for the non-integer case too provided that the term $\lambda(\omega)\pi$ in its statement is replaced by a general ambiguous phase term. This ambiguous term can be neglected if the spectral domination condition discussed before is satisfied. In this case, the TDOA estimation procedure is the same as before except that, now, the search for the D which maximizes the PHAT integral (6) should include non-integer values as well.

C. Choosing the sensor filters

In order to use the PHAT integral (6) as a valid estimator of D , one should use sensor filters $H_0(z)$ and $H_1(z)$ whose phase response satisfy the symmetry condition

$$\angle \left(H_0(e^{j\frac{\omega}{2}})H_1^*(e^{j\frac{\omega}{2}}) \right) = \angle \left(H_0(e^{j(\pi-\frac{\omega}{2})})H_1^*(e^{j(\pi-\frac{\omega}{2})}) \right) \quad (8)$$

required by Theorem 1. Several classes of filters satisfy (8). For instance, the reader may observe that if $H_0(z)$ and $H_1(z)$ are linear-phase, FIR and with the same length N , then $\angle H_0(e^{j\omega})H_1^*(e^{j\omega})$ becomes a constant which, in turn, implies (8). It is possible to satisfy (8) by using certain types of IIR filters as well. In the examples that follow, we present three representative choices for $H_0(z)$ and $H_1(z)$.

Example 2—Linear-phase FIR filters: Linear-phase FIR filters with good frequency selectivity can be designed using a variety of methods, most notably the weighted-Chebyshev method of Parks and McClellan [18]. In programming this method, an error function is formulated for the desired amplitude response in terms of a linear combination of cosine functions and is then minimized by using a very efficient multivariable optimization method known as the Remez exchange algorithm [19], [20, Ch. 15].

We used the MATLAB function `remez` which implements the Parks-McClellan algorithm to obtain a low-pass filter $H_0(z)$ with symmetric impulse response of length $N = 9$. A high-pass filter $H_1(z)$ of the same length whose amplitude response is the mirror-image of $H_0(z)$ was obtained by simply replacing z in $H_0(z)$ with $-z$. The amplitude responses of $H_0(z)$ and $H_1(z)$ are shown in Fig. 3(a) where their phase responses are depicted in Fig. 3(b). The amplitude and phase of $H_0(z)H_1^*(z)$ for the filters designed in this example are shown in Fig. 4 (a) and (b). As can be seen from Fig. 4(b), these filters satisfy the phase symmetry condition (8) perfectly. \diamond

Example 3—Bessel IIR filters: In general, it is not possible to achieve linear phase response with IIR filters. However, it is possible to design IIR low-pass and high-pass filters $H_0(z)$ and $H_1(z)$ such that the product $H_0(z)H_1^*(z)$ has linear phase. This can be achieved, for instance, using second-order Butterworth filters. Another approach is to design almost-linear-phase $H_0(z)$ and $H_1(z)$ by discretizing analog Bessel filters via the impulse-invariant transformation. Here, we opt for the latter approach.

For the purpose of this example, we used the MATLAB function `besself` to design an 8-order analog Bessel filter with cutoff frequency of 40Hz. Then, we discretized it using the MATLAB function `impinvar` at a sampling frequency of 20 Hz to obtain the low-pass filter $H_0(z)$. A high-pass filter $H_1(z)$ of the same order was obtained by replacing z in $H_0(z)$ with $-z$. The amplitude responses of $H_0(z)$ and $H_1(z)$

are shown in Fig. 3(c) where their phase responses are depicted in Fig. 3(d). The amplitude and phase of $H_0(z)H_1^*(z)$ for the Bessel filters designed in this example are shown in Fig. 4 (c) and (d). It is clear from Fig. 4(d) that $H_0(z)$ and $H_1(z)$ obey (8) with a good approximation. \diamond

Example 4—Perfect-reconstruction linear-phase FIR filters: Analysis/Synthesis filter banks for which it is possible to reconstruct the input signal (within a scale factor and a delay) are known as *perfect reconstruction* (PR) filter banks [5]. An interesting class of PR systems is based on linear-phase FIR filters. In this example, we use the filters $H_0(z) = 0.0091 + 0.7070z^{-1} + 0.7070z^{-2} + 0.0091z^{-3}$ and $H_1(z) = 0.0091 + 0.7070z^{-1} - 0.7070z^{-2} - 0.0091z^{-3}$ which belong to the PR class \mathcal{P}_1 introduced in Appendix III. The amplitude and phase responses of $H_0(z)$ and $H_1(z)$ are shown in Fig. 3 (e) and (f). The amplitude and phase response of the product filter $H_0(z)H_1^*(z)$ are shown in Fig. 4 (e) and (f). Clearly, $H_0(z)$ and $H_1(z)$ obey (8) perfectly. \diamond

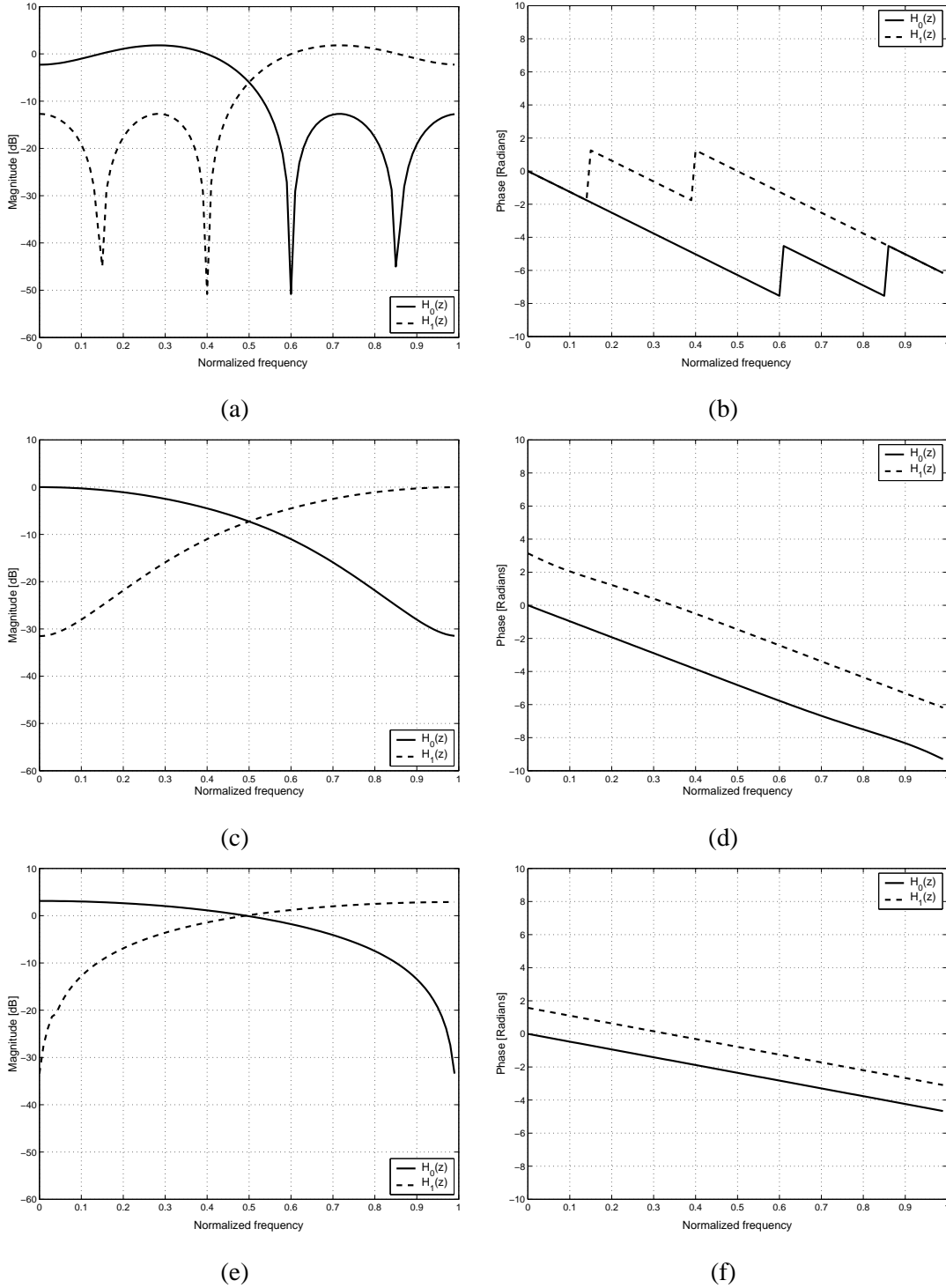


Fig. 3. Amplitude response and phase response of various sensor filters $H_0(z)$ and $H_1(z)$ introduced in Section II-C. (a) and (b): ordinary linear-phase FIR filters. (c) and (d): Bessel IIR filters. (e) and (f) perfect reconstruction linear-phase FIR filters.

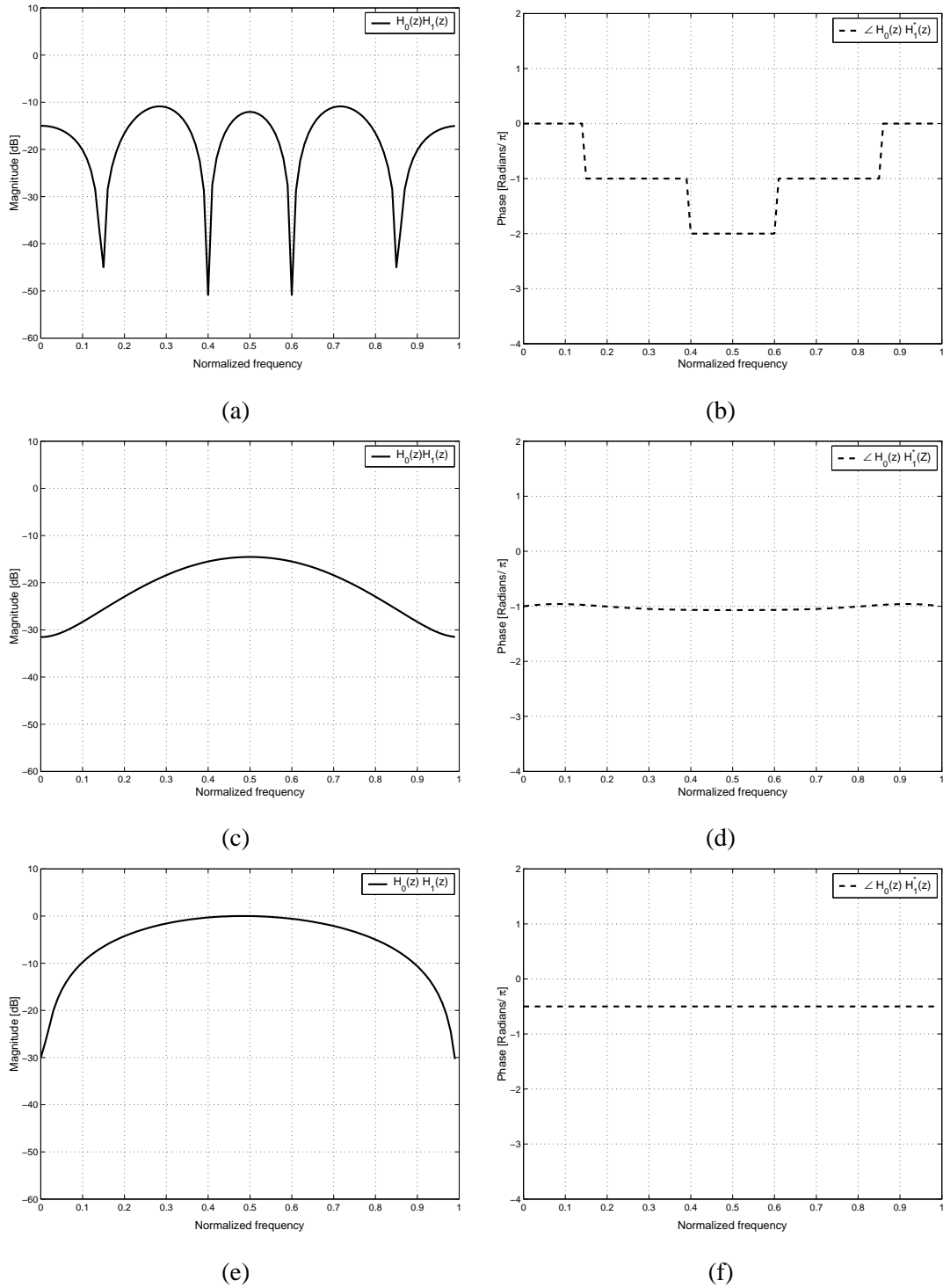
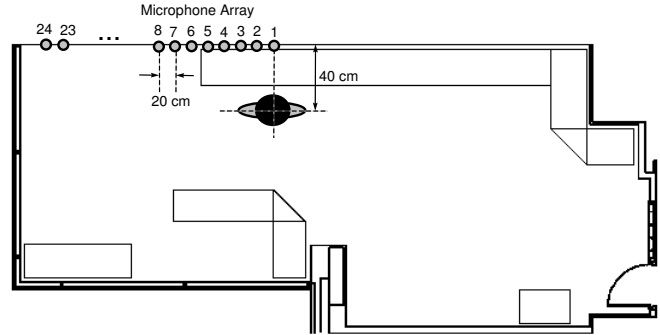


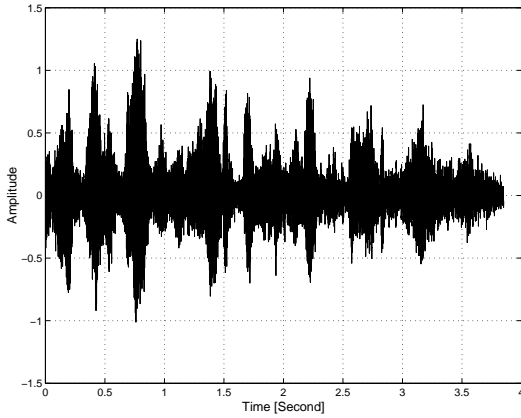
Fig. 4. Amplitude response and phase response of the product filter $H_0(z)H_1^*(z)$ for the sensor filters introduced in Section II-C. (a) and (b): ordinary linear-phase FIR filters. (c) and (d): Bessel IIR filters. (e) and (f) perfect reconstruction linear-phase FIR filters.



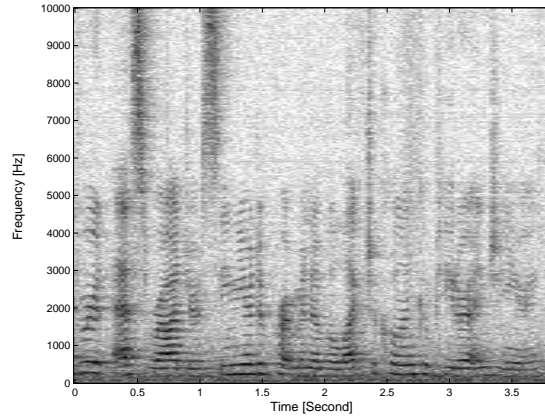
(a)



(b)



(c)



(d)

Fig. 5. (a), (b): The microphone array setup at the Artificial Perception Laboratory, University of Toronto. (c) The reference speech signal $x(n)$ recorded by Microphone No. 3 in the array. The array was receiving the voice of a female speaker saying the sentence “Edward S. Rogers Sr. Department of Electrical and Computer Engineering”. (d) The spectrogram of $x(n)$.

D. Multirate TDOA estimation experiments

In this section, we present actual multirate TDOA estimation experiments that support the theoretical results of Sections II-B and II-C. Our experimental setup is shown in Fig. 5(a) and (b). A female student spoke the sentence “Edward S. Rogers Sr. Department of Electrical and Computer Engineering” in front of a microphone array standing at the location specified in Fig. 5(b). The signal arriving at each microphone was sampled at 20 KHz and recorded for about 4 seconds.

We used only two microphones in the microphone array (No. 3 and No. 5). The output of microphone No. 3 was used as the reference signal $x(n)$. This signal and its spectrogram are shown in Fig. 5 (c) and (d), respectively. The signal recorded by microphone No. 5 was used as the second input. We used the example

analysis filters described in Section II-C to filter these signals and then down-sampled the results to obtain $v_0(n)$ and $v_1(n)$. An estimate $\hat{P}_{v_0v_1}(e^{j\omega})$ of the cross spectral density of the low-rate observations $v_0(n)$ and $v_1(n)$ was obtained by using the MATLAB function `csd`. This function estimates the cross spectral density of two signals using Welch’s averaged periodogram method (see, e.g., [16]). The parameters of the function `csd` were chosen such that it would operate as follows: First, the signals $v_0(n)$ and $v_1(n)$ were divided into overlapping sections of length 1024 and then each section was windowed by a von Hann window. The overlap length was set to 512. Several overlapping sections would form a “block”. The products of the DFTs of the sections of $v_0(n)$ and $v_0(n)$ which were in the same block were averaged to form $\hat{P}_{v_0v_1}(e^{j\omega})$ for that block. The block length was set to 4096.

The above procedure provided us with a short-time cross spectrum estimate for each block (4096 samples or about 0.4 seconds) of the low-rate measurements. We used this estimate to calculate the PHASE Transform integral

$$\int_{\omega} \cos \left(-D \frac{\omega}{2} - (\angle \hat{P}_{v_0v_1}(e^{j\omega}) - \angle W(e^{j\frac{\omega}{2}})) \right) d\omega. \quad (9)$$

for each block and for all delay values D from -40 to 40. This process, which we call short-time PHASE Transform, was repeated until all the blocks in the signals $v_0(n)$ and $v_0(n)$ were covered. In Fig. 6, we have used shades of gray to depict the numerical value of the integral in (9) for all blocks in the signals $v_0(n)$ and $v_0(n)$ and for $-40 \leq D \leq 40$. For each block, the D value which maximizes the integral in (9) (i.e. the one which has produced the brightest color) represents the time delay estimate \hat{D} for that block. Fig. 6 also shows the value of the integral (8) as a function of D averaged over the entire length of the signals $v_0(n)$ and $v_0(n)$. The D value which maximizes this quantity represents the TDOA estimate for the entire signal³. The plots in Fig. 6 show that $\hat{D} = 13$. This value was validated with estimates obtained from the original (full-rate) microphone signals.

Remark 3: Note that the in the above experiments, the TDOA value is odd which means the phase of $P_{v_0v_1}(e^{j\omega})$ contains the ambiguous component $\lambda(\omega)\pi$. Recall that in the odd TDOA case, the PHAT estimator is guaranteed to work only if the spectrum dominance condition mentioned in Section II-B is satisfied. This condition is not satisfied for the blocks centered at $t = 0.5$, $t = 1$ and $t = 2.75$ since these blocks contain strong components in both high and low frequencies (see Fig. 5(d)). The short-time PHAT plots in Fig. 6 (a) and (c) do not show a prominent peak for these blocks. This indicates the failure of the PHAT-based TDOA estimation for these blocks in agreement with our theory.

³Of course this assumes that D remains constant during the recording.

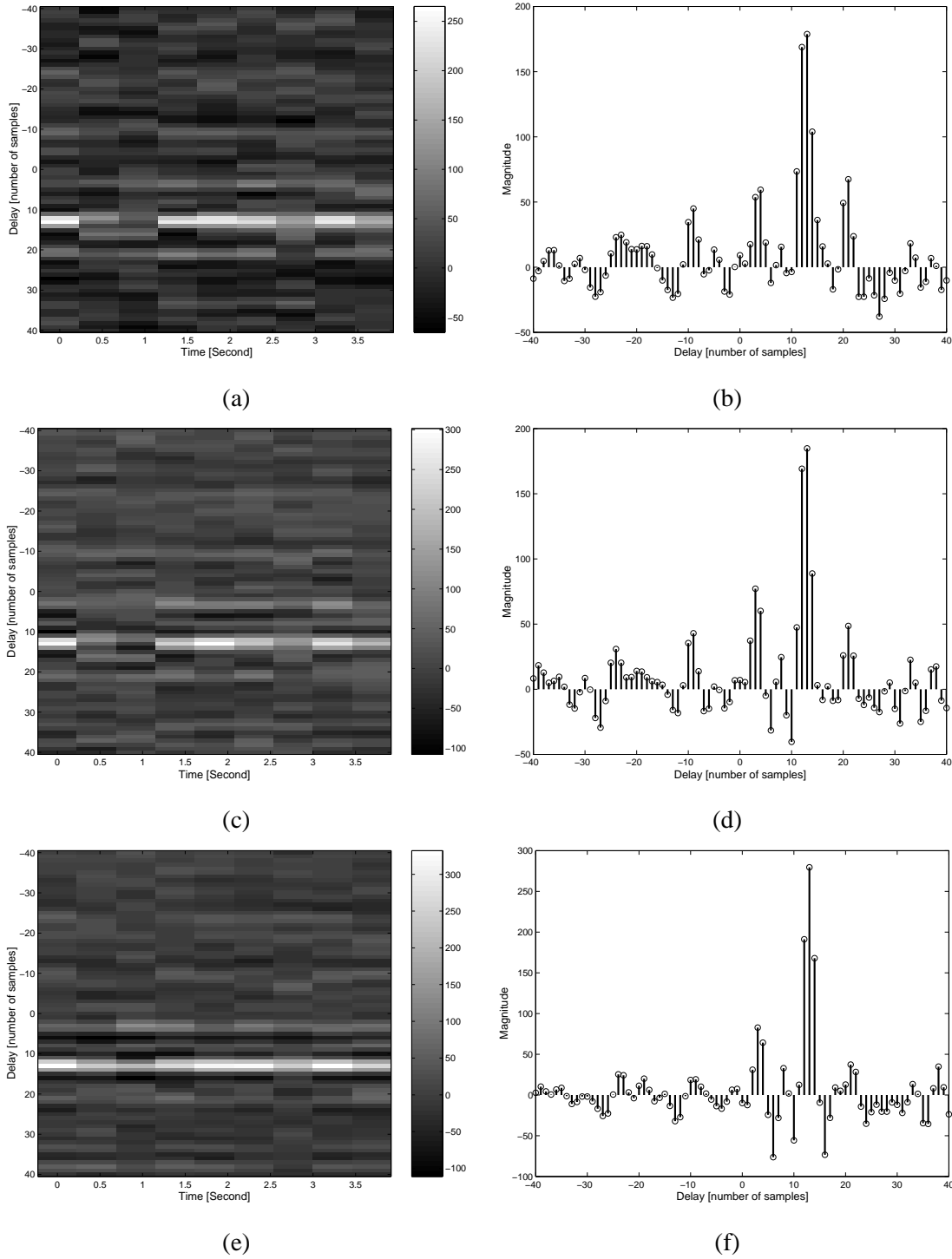


Fig. 6. TDOA estimation results using the filters $H_0(z)$ and $H_1(z)$ described in Section II-C. Each row shows Short-time PHASE Transform results in the left and PHASE Transform averaged over the entire signal on the right. (a) and (b): ordinary linear-phase FIR filters. (c) and (d): Bessel IIR filters. (e) and (f) perfect reconstruction linear-phase FIR filters.

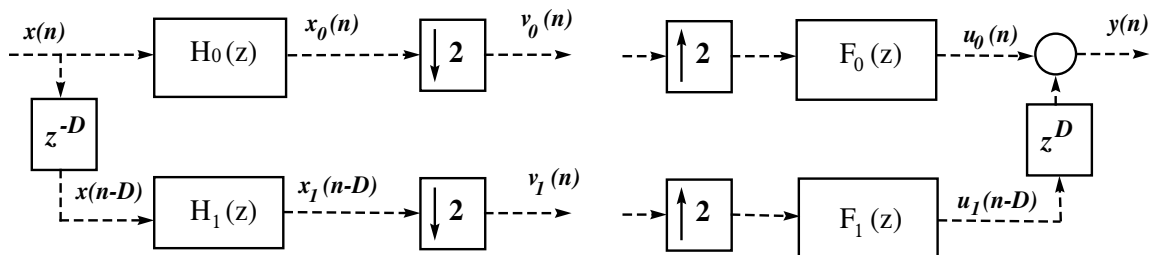


Fig. 7. Reconstructing a high-rate measurement using a standard synthesis filter bank equipped with an advance block z^D to compensate for the TDOA.

III. FUSION OF LOW-RATE SIGNALS IN THE PRESENCE OF TIME DELAY

In this section we focus on the second fundamental problem of multirate sensor array design (Problem 2, Section I). Except from the delay block z^{-D} , the sensor model shown in Fig 2 is a standard two-channel analysis filter bank. It seems reasonable, therefore, to use a standard synthesis filter bank equipped with a compensating *advance block* z^D to reconstruct the signal $x(n)$ from the low-rate signals $v_i(n)$ (Fig 7).

Theorem 2: The multirate analysis/synthesis system shown in Fig 7 can achieve perfect reconstruction for all values of D only if

$$H_0(e^{j\omega}) = F_0(e^{j\omega}) = 0, \quad \forall \omega \in \Omega$$

$$H_1(e^{j\omega}) = F_1(e^{j\omega}) = 0, \quad \forall \omega \in \hat{\Omega}$$

where $\Omega = [0 \frac{\pi}{2})$ and $\hat{\Omega} = (\frac{\pi}{2} \pi]$ or the other way around.

Proof: See Appendix II. ■

Unfortunately, the frequency responses that satisfy the conditions of Theorem 2 can not be realized using FIR or IIR structures⁴. In practical terms, this means it is not possible to achieve perfect reconstruction for *all* TDOA values by using a fixed pair of synthesis filters in the structure shown in Fig 7. One, therefore, has to use different pairs of synthesis filters for different TDOA values.

Let's write the TDOA D as $D = 2K + \tilde{D}$ where $K \in \mathbb{Z}$ and $\tilde{D} \in [0, 2)$. In this case, the delay block in the sensors' filter bank model (Fig. 2) can be decomposed into an integer, even, delay z^{-2K} and a residual delay $z^{-\tilde{D}}$. z^{-2K} commutes with down-sampling and up-sampling operation. Thus, it can be readily compensated for in the receiving end by adding an equivalent delay z^{-2K} to the other channel. The

⁴Note that realizable filters have rational transfer functions which can have only a finite number of transmission zeros in their frequency response. Theorem 2, however, requires zero response over a continuous range of frequencies.

residual part $z^{-\tilde{D}}$, however, does not commute with the down-sampling or up-sampling blocks. Thus, when designing the fusion system, we have to consider it along with the filter $H_1(z)$ in Fig. 7. In other words, $H_1(z)$ subsumes $z^{-\tilde{D}}$ as shown in Fig. 8.

When \tilde{D} is different from 0 or 1, the transfer function $z^{-\tilde{D}}$ cannot be realized using a finite-order physical system. In this case, one must approximate $z^{-\tilde{D}}$ by a finite-order rational transfer function. This can be done by using the classic Padé approximation [21] or other more recent techniques [22], [23].

Once $z^{-\tilde{D}}$ is approximated and combined with $H_1(z)$, a synthesis filter bank must be designed to reconstruct $x(n)$ (Fig. 8). The synthesis filters $F_0(z)$ and $F_1(z)$ depend on \tilde{D} . Thus, they must be designed (in real time if needed) after the TDOA D is estimated.

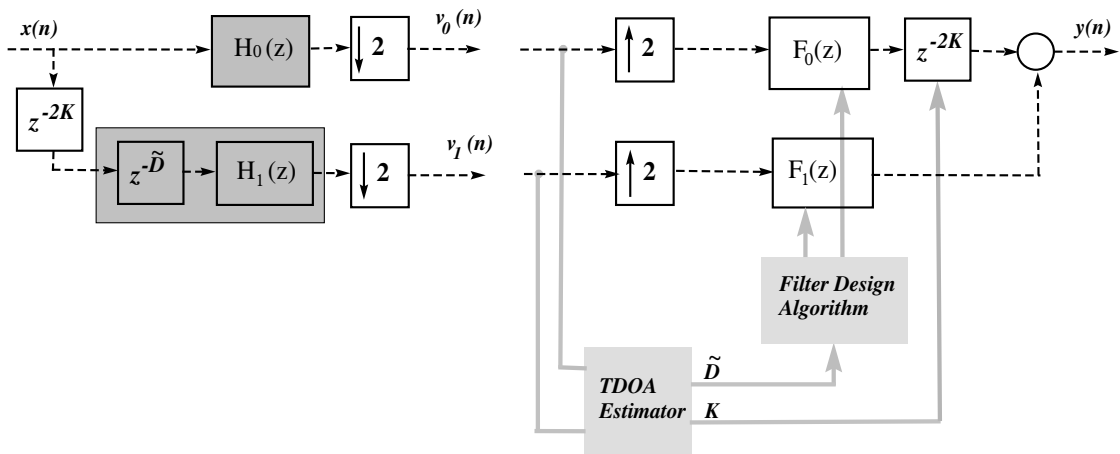


Fig. 8. The structure of the central fusion system along with the analysis filter bank model used for designing $F_0(z)$ and $F_1(z)$.

IV. DESIGNING THE SYNTHESIS FILTERS

The synthesis filters in Figs. 8 should be designed such that the reconstructed signal $y(n)$ resembles the desired reference signal $x(n)$ as closely as possible (within, perhaps, a scale factor and a delay). An efficient way to do this is the model-matching technique first proposed by Shenoy [24], [25] in the context of multirate systems. Here, we use an elegant variation of the model-matching approach due to Chen and Francis [26]. These authors used \mathcal{H}_∞ optimization theory to minimize the ℓ_2 -induced norm between a pure delay system and the multirate system at hand. A version of the \mathcal{H}_∞ optimization method which uses linear matrix inequalities (LMIs) and achieves reduced-order solutions has been recently proposed by Li and Kok [27].

A. Synthesis filter bank design using \mathcal{H}_∞ optimization

\mathcal{H}_∞ optimization is central in modern control theory [28], [29], [30]. The Hardy space \mathcal{H}_∞ consists of all complex-valued functions $H(z)$ that are analytic and bounded outside the unit disc, that is $|z| > 1$. Therefore, \mathcal{H}_∞ is the space of transfer functions of causal and LTI systems which are stable in the bounded-input, bounded-output (BIBO) sense. The norm of a multi-input multi-output transfer function $\mathbf{H}(z) \in \mathcal{H}_\infty$ is defined as the peak magnitude of its maximum singular value on the unit circle:

$$\|\mathbf{H}\|_\infty \triangleq \sup_{\omega} \sigma_{max}[\mathbf{H}(e^{j\omega})]. \quad (10)$$

If $\mathbf{H}(z)$ is the transfer function of a stable, causal LTI system with input $X(n)$ of dimension m and output $Y(n)$ of dimension p , so that $\mathbf{H}(z)$ is $p \times m$, then the induced norm from the input space ℓ_2^m to the output space ℓ_2^p equals the \mathcal{H}_∞ -norm of $\mathbf{H}(z)$. That is,

$$\sup_{\|X\|_2=1} \|Y\|_2 = \|\mathbf{H}\|_\infty \quad (11)$$

where the norm of a signal $X(n)$ in ℓ_2^m is defined to be

$$\|X\|_2 \triangleq \left(\sum_n X^T(n)X(n) \right)^{\frac{1}{2}}. \quad (12)$$

Now, consider the analysis/synthesis filter bank shown in Fig. 8. Because of the down-sampling and up-sampling operations, the system which relates the output signal $y(n)$ to the input signal $x(n)$ is, in general, a linear periodically time-varying (LPTV) system. Thus, it does not admit a transfer function. However, we can “block” the input and output signals to obtain an LTI input-output equivalent system. This latter system has the two-dimensional input and output

$$X(n) \triangleq \begin{bmatrix} x(2n) & x(2n+1) \end{bmatrix}^T, \quad Y(n) \triangleq \begin{bmatrix} y(2n) & y(2n+1) \end{bmatrix}^T \quad (13)$$

and a 2×2 transfer matrix which we denote by $\mathbf{P}(z)$.

To find an expression for $\mathbf{P}(z)$, we have to use the *polyphase representation* [5] of the analysis and synthesis filters. Let us represent the analysis filters $H_0(z)$ and $H_1(z)$ compactly by defining the transfer vector $\mathbf{h}(z) \triangleq [H_0(z) \ H_1(z)]^T$. It is possible to factor $\mathbf{h}(z)$ as the product of a 2×2 transfer matrix $\mathbf{E}(z)$ and a delay vector $\mathbf{e}(z)$. That is,

$$\mathbf{h}(z) = \mathbf{E}(z^2)\mathbf{e}(z) \quad (14)$$

where $\mathbf{e}(z) \triangleq [1 \ z^{-1}]^T$. The matrix $\mathbf{E}(z)$ is called the *type-1 polyphase matrix* associated with the analysis filter bank $\mathbf{h}(z)$. Similarly, the synthesis filters can be represented in the compact form $\mathbf{f}(z) \triangleq [F_0(z) \ F_1(z)]$ which, in turn, may be factored as

$$\mathbf{f}(z) \triangleq \mathbf{e}^T(z) \mathbf{R}(z^2). \quad (15)$$

The matrix $\mathbf{R}(z)$ is called a *type-2 polyphase matrix*. Using the polyphase notation, it is straightforward to show that

$$\mathbf{P}(z) \triangleq \mathbf{R}(z) \mathbf{E}(z). \quad (16)$$

Our objective is to design the synthesis filters $F_0(z)$ and $F_1(z)$ given the analysis filters $H_0(z)$ and $H_1(z)$, and a tolerable delay $T_d \in \mathbb{Z}_+$ such that $y(n)$ is “as close as possible” to $x(n - T_d)$. This objective can be made precise by defining the *error signal* $e(n) \triangleq y(n) - x(n - T_d)$ and then minimizing the *performance measure*

$$J \triangleq \sup_{\|x\|=1} \|e\|_2 \quad (17)$$

which measures the worst-case ℓ_2 -induced norm from the input signal $x(n)$ to $e(n)$. Blocking preserves ℓ_2 norm, that is, the norm of a signal in ℓ_2 is equal to the norm of its blocked version in ℓ_2^m . Using this fact and (11), it can be shown that [26, Theorem 2.1]

$$J = \|\mathbf{C} - \mathbf{R}\mathbf{E}\|_\infty \quad (18)$$

where

$$\mathbf{C}(z) \triangleq \begin{cases} z^{-k} \begin{bmatrix} 1 & 0 \\ 0 & 1 \end{bmatrix}, & \text{if } T_d = 2k + 1, \\ z^{-k} \begin{bmatrix} 0 & z \\ 1 & 0 \end{bmatrix}, & \text{if } T_d = 2k. \end{cases} \quad (19)$$

Based on the above result, our design problem can be precisely stated as follows: Given causal and stable (FIR or IIR) analysis filters $H_0(z)$ and $H_1(z)$ and given a tolerable overall delay T_d , find causal, stable IIR synthesis filters $F_0(z)$ and $F_1(z)$ such that J is minimized. The optimum performance measure J_{opt} is therefore

$$J_{opt} = \inf_{F_0(z), F_1(z)} \sup_{\|x\|=1} \|e\|_2 = \inf_{\mathbf{R}(z) \in \mathcal{H}_\infty} \|\mathbf{C} - \mathbf{R}\mathbf{E}\|_\infty. \quad (20)$$

The latter optimization is a standard \mathcal{H}_∞ model matching problem and can be solved using existing software tools, e.g. the μ -Analysis and Synthesis Toolbox of MATLAB. For reader’s convenience, the \mathcal{H}_∞ -optimal synthesis filter design procedure is outlined in Algorithm 1.

Algorithm 1: \mathcal{H}_∞ -optimal synthesis filter design

Input: The analysis filters $H_0(z)$ and $H_1(z)$, and the tolerable system delay T_d .

Output: The synthesis filters $F_0(z)$ and $F_1(z)$, and the worst-case reconstruction error J_{opt} .

Procedure:

1. Construct the polyphase matrix $\mathbf{E}(z)$ associated with the analysis filters $H_0(z)$ and $H_1(z)$.
2. Construct the delay matrix

$$\mathbf{C}(z) \triangleq \begin{cases} z^{-k} \begin{bmatrix} 1 & 0 \\ 0 & 1 \end{bmatrix}, & \text{if } T_d = 2k + 1, \\ z^{-k} \begin{bmatrix} 0 & z \\ 1 & 0 \end{bmatrix}, & \text{if } T_d = 2k. \end{cases}$$

3. Find $\mathbf{R}_{opt}(z) \in \mathcal{H}_\infty$ which minimizes $J = \|\mathbf{C} - \mathbf{R}\mathbf{E}\|_\infty$.
4. Return $[F_0(z) \ F_1(z)] = \mathbf{e}^T(z)\mathbf{R}_{opt}(z^2)$.
5. Return $J_{opt} = \|\mathbf{C} - \mathbf{R}_{opt}\mathbf{E}\|_\infty$.

The MATLAB function that solves the \mathcal{H}_∞ optimization in Step 3 of Algorithm 1 is `hinfsyn`. To apply this function one has to reformulate the model matching problem at hand as a continuous-time \mathcal{H}_∞ controller design problem in the state-space. The solution is calculated as a continuous-time state-space realization as well. This realization must be converted to the transfer matrix format and discretized to produce $\mathbf{R}_{opt}(z)$. Details of this process are described in [26, Section III].

The order of the transfer matrix $\mathbf{R}_{opt}(z)$ depends on the dimension of the state-space models supplied for $\mathbf{E}(z)$ and $\mathbf{C}(z)$. In practice, the state space models for $\mathbf{E}(z)$ and $\mathbf{C}(z)$ tend to have high dimensions, resulting in high-order solutions for $\mathbf{R}_{opt}(z)$ and, in turn, synthesis filters $H_i(z)$ of unacceptably high order. To circumvent this difficulty, we used the MATLAB function `sysbal`⁵ to calculate a truncated (reduced order) realization of the state-space solution provided by `hinfsyn`. The resulting reduced-order model was then discretized and converted to the transfer matrix format to get $\mathbf{R}_{opt}(z)$.

⁵This function calculates the optimal (in the sense of minimum Hankel norm) truncated approximation to a system model. We used the recommended (default) values for the approximation error. See the μ -Analysis and Synthesis Toolbox User's Guide for details.

B. Example designs for the integer TDOA case

In the special case that D assumes integer values only, two pairs of synthesis filters are sufficient for all TDOA circumstances. This is because, in this case, \tilde{D} is either 0 or 1. Here, we provide three design examples for this simple case assuming that the sensor filters are those designed in Section II-C.

The \mathcal{H}_∞ -optimal synthesis filters $F_0(z)$ and $F_1(z)$ (designed for even- and odd-TDOA values separately) are shown in Fig. 9. The total system delay T_d which was chosen for each case is also quoted in this figure. The worst-case reconstruction error norm J_{opt} for the synthesis filter bank pairs depicted in Fig. 9 are shown in Table I.

The figures reported in Table I are quite impressive once we note that the reconstruction error norm J_{opt} represents *the worst-case scenario* and the actual reconstruction error for a concrete case can be much less. Moreover, the reader is reminded that the peak reconstruction error J_{opt} depends on both the analysis filters and the value chosen for T_d . In general, J_{opt} decreases as T_d increases. Graphic depictions of this phenomenon can be found in Chen and Francis [26]. These authors also prove the predictable result that if the polyphase matrix $\mathbf{E}(e^{j\omega})$ is nonsingular for all ω , then $\lim_{T_d \rightarrow \infty} J_{opt} = 0$. In this case, arbitrary good reconstruction would be possible if a sufficiently large time delay is tolerated⁶. In our experiments, we were able to achieve $J_{opt} \leq -80\text{dB}$ for all the example analysis filter banks introduced in Section II-C by choosing a large enough T_d .

TABLE I

WORST-CASE RECONSTRUCTION ERROR NORM J_{opt} FOR THE OPTIMAL SYNTHESIS FILTERS SHOWN IN FIG. 9.

| Type of analysis filters | J_{opt} for even TDOA values | J_{opt} for odd TDOA values |
|---|--------------------------------|-------------------------------|
| ordinary linear-phase FIR | -70.4 dB | -65.3 dB |
| Bessel IIR | - 54.6 dB | less than -80 dB |
| Perfect Reconstruction linear-phase FIR | less than -80 dB | less than -80 dB |

⁶Note that $\mathbf{E}(e^{j\omega})$ depends on the actual TDOA. So, $\mathbf{E}(e^{j\omega})$ might become singular for some D even if $H_i(z)$ were originally chosen to be perfect reconstruction.

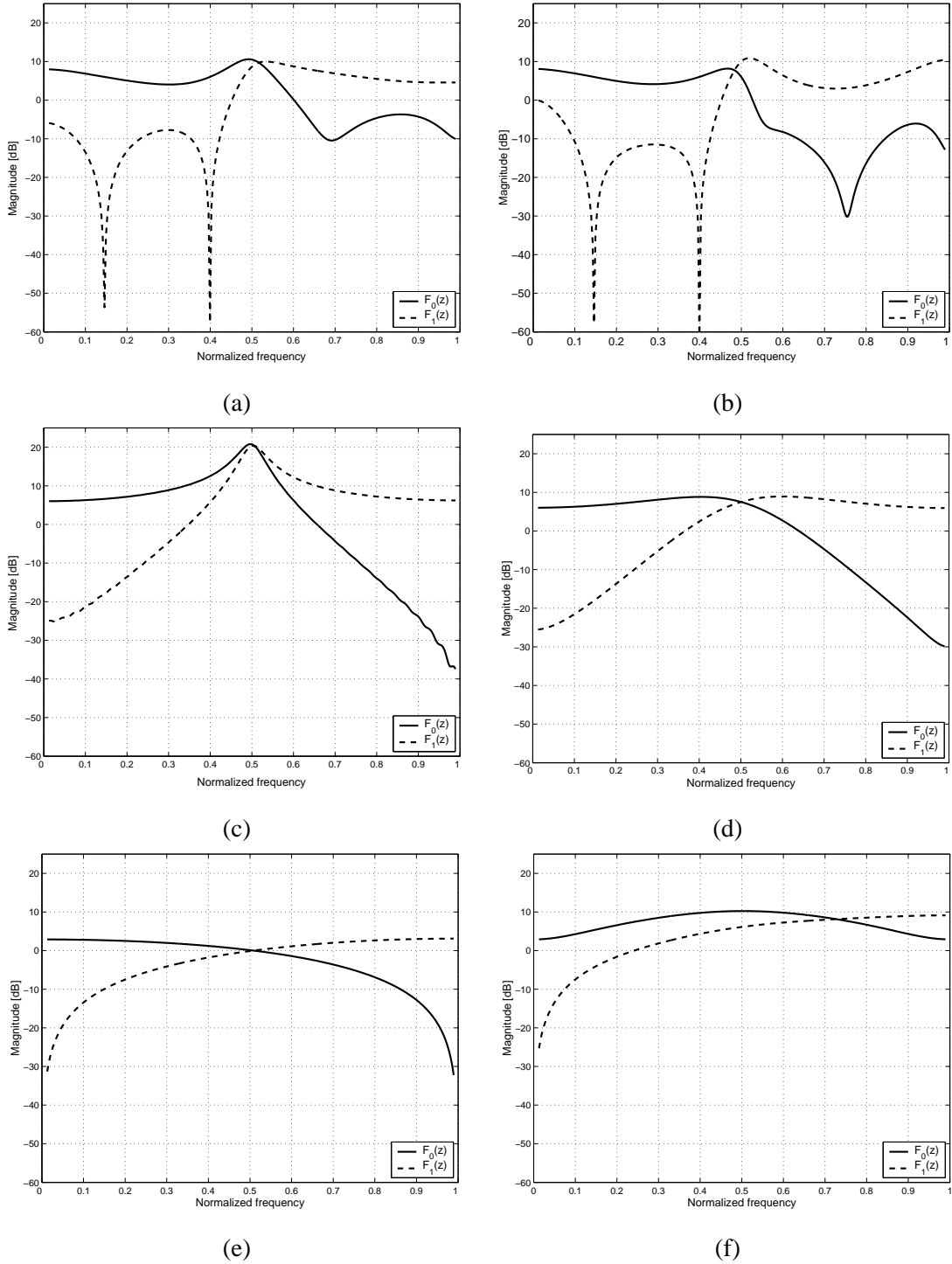


Fig. 9. \mathcal{H}_∞ optimal synthesis filters designed for each pair of analysis filters introduced in the design examples of Section II-C. The right hand plot in each row shows the synthesis filters $F_i(z)$ used for even TDOA values while those on the left are $G_i(z)$ used for odd TDOA values. (a) and (b): ordinary linear-phase FIR analysis filters, $T_d = 27$ samples. (c) and (d): Bessel IIR analysis filters, $T_d = 35$ samples. (e) and (f) Perfect Reconstruction linear-phase FIR analysis filters, $T_d = 7$ samples.

V. PROCEDURE FOR DESIGNING MULTIRATE SENSOR ARRAYS

Based on the results presented in the previous sections, the following procedure is suggested for designing multirate sensor arrays:

1. Choose a pair of filters $H_0(z)$ and $H_1(z)$ such that their frequency response satisfy the symmetry condition

$$\angle \left(H_0(e^{j\frac{\omega}{2}})H_1^*(e^{j\frac{\omega}{2}}) \right) = \angle \left(H_0(e^{j(\pi-\frac{\omega}{2})})H_1^*(e^{j(\pi-\frac{\omega}{2})}) \right)$$

required by Theorem 1.

2. Perform TDOA estimation experiments using the PHAT estimator

$$\hat{D} = \arg \max_D \int_{\omega} \cos \left(-D \frac{\omega}{2} - (\angle \hat{P}_{v_0 v_1}(e^{j\omega}) - \angle H_0(e^{j\frac{\omega}{2}})H_1^*(e^{j\frac{\omega}{2}})) \right) d\omega$$

and see whether the results are consistent and accurate.

3. Choose a $\tilde{D} \in [0, 2)$ randomly. Then, choose a value for the tolerable overall delay T_d and use Algorithm 1 to design the synthesis filters $F_i(z)$, $i = 1, 2$, for the analysis filters selected in Step 1. Record the worst-case reconstruction error gain J_{opt} .
4. Choose as many different $\tilde{D} \in [0, 2)$ as possible and repeat Step 3. If steps 2 or 3 do not produce satisfactory results, then choose a different pair of analysis filters in Step 1 and repeat the procedure.

VI. CONCLUDING REMARKS

We studied the theory and design of multirate sensor arrays. We showed that the following are the fundamental problems involved: a) How to extend TDOA estimation techniques to multirate signals? and b) How to design analysis and synthesis filters which allow signal fusion when TDOA is present? We posed and solved these problems by reference to a simple model involving only two sensors. We believe that our work is novel in the sense that, to the best of our knowledge, it is the first to address fusion of low-resolution sensors in the presence of TDOA. It is, however, intended as an initial theory. Important issues such as robustness of the low-rate PHAT estimator, M -channel systems with $M > 2$, and how to specify “the best choice” for sensor filters are left for future research.

As Einstein has said it, “No fairer destiny could be allotted to any theory than that it should itself point out the way to introducing a more comprehensive theory in which it lives on as a limiting case.” Theory of multirate sensors is an emerging research area. We hope our results point out the way towards more complete theories and help to give shape to this emerging field.

APPENDIX I

PROOF OF THEOREM 1

Consider the diagram shown in Fig. 2. It is straightforward to verify that the output signals $v_0(n)$ and $v_1(n)$ are jointly wide-sense stationary (see, for example, [31]). Thus, the cross-correlation function $R_{v_0v_1}(k)$ defined by

$$R_{v_0v_1}(k) \triangleq E\{v_0(n)v_1(n+k)\} \quad (21)$$

exists. The signals $v_0(n)$ and $v_1(n)$ are down-sampled versions of $x_0(n)$ and $x_1(n-D)$. That is, $v_0(n) = x_0(2n)$ and $v_1(n) = x_1(2n-D)$. Thus we have

$$\begin{aligned} R_{v_0v_1}(k) &= E\{x_0(2n)x_1(2n+2k-D)\} \\ &= R_{x_0x_1}(2k-D). \end{aligned} \quad (22)$$

The above equation allows us to express the CSD $P_{v_0v_1}(e^{j\omega})$ of the low-rate signals in terms of the CSD $P_{x_0x_1}(e^{j\omega})$ associated with $x_0(n)$ and $x_1(n)$:

$$\begin{aligned} P_{v_0v_1}(e^{j\omega}) &\triangleq \sum_{k=-\infty}^{\infty} R_{v_0v_1}(k)e^{-j\omega k} \\ &= \sum_{k=-\infty}^{\infty} R_{x_0x_1}(2k-D)e^{-j\omega k} = \frac{1}{2}e^{-j\omega\frac{D}{2}} \times \end{aligned} \quad (23)$$

$$\begin{cases} P_{x_0x_1}(e^{j\frac{\omega}{2}}) + P_{x_0x_1}(e^{j\frac{\omega-2\pi}{2}}) & D \text{ even} \\ P_{x_0x_1}(e^{j\frac{\omega}{2}}) - P_{x_0x_1}(e^{j\frac{\omega-2\pi}{2}}) & D \text{ odd} \end{cases}$$

In the last step of the above derivations we used the following properties of the discrete-time Fourier transform:

$$x(n) \xrightarrow{\mathcal{F}} X(e^{j\omega}) \Rightarrow \begin{cases} x(2n) & \xrightarrow{\mathcal{F}} \frac{X(e^{j\frac{\omega}{2}}) + X(e^{j\frac{\omega-2\pi}{2}})}{2} \\ x(n-D) & \xrightarrow{\mathcal{F}} e^{-j\omega D} X(e^{j\omega}) \end{cases}$$

It is straightforward to show that

$$P_{x_0x_1}(e^{j\omega}) = W(e^{j\omega})P_{xx}(e^{j\omega}), \quad (24)$$

where $P_{xx}(e^{j\omega})$ is the power spectral density (PSD) of the input signal. It follows from (23) and (24) that

$$\angle P_{v_0v_1}(e^{j\omega}) = \begin{cases} -D\frac{\omega}{2} + \angle \left(P_{xx}(e^{j\frac{\omega}{2}})W(e^{j\frac{\omega}{2}}) + P_{xx}(e^{j\frac{\omega-2\pi}{2}})W(e^{j\frac{\omega-2\pi}{2}}) \right) & D \text{ even} \\ -D\frac{\omega}{2} + \angle \left(P_{xx}(e^{j\frac{\omega}{2}})W(e^{j\frac{\omega}{2}}) - P_{xx}(e^{j\frac{\omega-2\pi}{2}})W(e^{j\frac{\omega-2\pi}{2}}) \right) & D \text{ odd} \end{cases}$$

The PSD of a real-valued WSS process is a real and positive function of frequency. Thus, $\angle P_{xx}(e^{j\omega}) = 0$. If the condition $\angle W(e^{j\frac{\omega}{2}}) = \angle W(e^{j\frac{\omega-2\pi}{2}})$ holds, we can simplify the above equation to get

$$\angle P_{v_0 v_1}(e^{j\omega}) = \begin{cases} -D\frac{\omega}{2} + \angle W(e^{j\frac{\omega}{2}}) & D \text{ even} \\ -D\frac{\omega}{2} + \angle W(e^{j\frac{\omega}{2}}) + \angle \left(P_{xx}(e^{j\frac{\omega}{2}}) \left| W(e^{j\frac{\omega}{2}}) \right| - P_{xx}(e^{j\frac{\omega-2\pi}{2}}) \left| W(e^{j\frac{\omega-2\pi}{2}}) \right| \right) & D \text{ odd} \end{cases}$$

In the above expression, the terms within the brackets are real. Thus, the phase contribution of the bracketed terms is either zero or π .

APPENDIX II

PROOF OF THEOREM 2

Consider the block diagram shown in Fig. 7. When $x(n) \in \ell_2$, the Fourier transforms $V_0(e^{j\omega})$ and $V_1(e^{j\omega})$ of the low-rate signals $v_1(n)$ and $v_2(n)$ exist and can be expressed as

$$\begin{aligned} V_0(e^{j\omega}) &= \frac{1}{2} [H_0(e^{j\frac{\omega}{2}})X(e^{j\frac{\omega}{2}}) + H_0(e^{j\frac{\omega-2\pi}{2}})X(e^{j\frac{\omega-2\pi}{2}})], \\ V_1(e^{j\omega}) &= \frac{1}{2} [e^{-j\frac{\omega}{2}D}H_1(e^{j\frac{\omega}{2}})X(e^{j\frac{\omega}{2}}) + e^{-j\frac{\omega-2\pi}{2}D}H_1(e^{j\frac{\omega-2\pi}{2}})X(e^{j\frac{\omega-2\pi}{2}})]. \end{aligned}$$

The Fourier transforms $U_0(e^{j\omega})$ and $U_1(e^{j\omega})$ of the synthesized signals $u_0(n)$ and $u_1(n)$ can be written as

$$\begin{aligned} U_0(e^{j\omega}) &= F_0(e^{j\omega})V_0(e^{j2\omega}), \\ U_1(e^{j\omega}) &= e^{j\omega D}F_1(e^{j\omega})V_1(e^{j2\omega}). \end{aligned}$$

Finally, $Y(e^{j\omega}) = U_0(e^{j\omega}) + U_1(e^{j\omega})$. It is straightforward to combine the previous four equations and express $Y(e^{j\omega})$ in terms of the *true spectrum* $X(e^{j\omega})$ and the *image spectrum* $X(e^{j(\pi-\omega)})$ as follows

$$Y(e^{j\omega}) = \frac{1}{2}A(e^{j\omega})X(e^{j\omega}) + \frac{1}{2}B(e^{j\omega})X(e^{j(\pi-\omega)});$$

where

$$\begin{aligned} A(e^{j\omega}) &\triangleq [F_0(e^{j\omega})H_0(e^{j\omega}) + F_1(e^{j\omega})H_1(e^{j\omega})], \\ B(e^{j\omega}) &\triangleq [F_0(e^{j\omega})H_0(e^{j(\pi-\omega)}) + e^{j\pi D}F_1(e^{j\omega})H_1(e^{j(\pi-\omega)})]. \end{aligned}$$

A necessary condition for perfect reconstruction is that terms pertaining to the image spectrum $X(e^{j(\pi-\omega)})$ are completely eliminated in the output. That is $B(e^{j\omega}) = 0$. Another necessary condition is that $A(e^{j\omega})$ becomes a non-zero constant. The condition that $B(e^{j\omega}) = 0$ is possible for all values of $D \in \mathbb{Z}$ only if

both $F_0(e^{j\omega})H_0(e^{j(\pi-\omega)}) = 0$ and $F_1(e^{j\omega})H_1(e^{j(\pi-\omega)}) = 0$ for all ω . To satisfy the latter condition, the products $F_0(e^{j\omega})H_0(e^{j\omega})$ and $F_1(e^{j\omega})H_1(e^{j\omega})$ should not vanish simultaneously. Using logical notation we can write these necessary conditions in the compact form:

$$F_0(e^{j\omega})H_0(e^{j\omega}) = 0 \quad \text{XOR} \quad F_1(e^{j\omega})H_1(e^{j\omega}) = 0 \quad (25)$$

$$F_0(e^{j\omega})H_0(e^{j(\pi-\omega)}) = 0 \quad \text{AND} \quad F_1(e^{j\omega})H_1(e^{j(\pi-\omega)}) = 0 \quad (26)$$

Let $\Gamma \triangleq [0 \frac{\pi}{2}) \cup (\frac{\pi}{2} \pi]$. Denote by Ω the set of all frequencies in Γ for which $F_0(e^{j\omega})$ is identically zero and define $\bar{\Omega} \triangleq \Gamma - \Omega$. In other words, assume

$$F_0(e^{j\omega}) \triangleq 0, \quad \omega \in \Omega, \quad (27)$$

$$F_0(e^{j\omega}) \neq 0, \quad \omega \in \bar{\Omega}. \quad (28)$$

It follows from (25) that the synthesis filters $F_0(e^{j\omega})$ and $F_1(e^{j\omega})$ cannot vanish at the same frequencies. They cannot be both nonzero at the same frequency either. The reason is that if they become nonzero at the some frequencies, (26) will require that $H_0(e^{j(\pi-\omega)})$ and $H_1(e^{j(\pi-\omega)})$ both be zero at those frequencies. This implies that $H_0(e^{j\omega})$ and $H_1(e^{j\omega})$ will vanish simultaneously and therefor contradicts (25). Thus, in summary, $F_1(e^{j\omega})$ should vanish wherever $F_0(e^{j\omega})$ is nonzero and vice versa:

$$F_1(e^{j\omega}) \neq 0, \quad \omega \in \Omega, \quad (29)$$

$$F_1(e^{j\omega}) = 0, \quad \omega \in \bar{\Omega}. \quad (30)$$

To satisfy (27)-(30) along with the original conditions in (25) and (26), it is further required that

$$H_1(e^{j\omega}) \neq 0 \quad \text{AND} \quad H_1(e^{j(\pi-\omega)}) = 0, \quad \omega \in \Omega, \quad (31)$$

$$H_0(e^{j\omega}) \neq 0 \quad \text{AND} \quad H_0(e^{j(\pi-\omega)}) = 0, \quad \omega \in \bar{\Omega}. \quad (32)$$

The above conditions can be satisfied only if

$$\omega \in \Omega \implies \pi - \omega \in \bar{\Omega} \quad \text{AND} \quad \omega \in \bar{\Omega} \implies \pi - \omega \in \Omega \quad (33)$$

which is possible only if $\Omega = [0 \frac{\pi}{2})$ or $\Omega = (\frac{\pi}{2} \pi]$. Thus, to satisfy (31) and (32) simultaneously it is required that $\Omega = [0 \frac{\pi}{2})$, $\bar{\Omega} = (\frac{\pi}{2} \pi]$ or $\bar{\Omega} = [0 \frac{\pi}{2})$, $\Omega = (\frac{\pi}{2} \pi]$ and that

$$H_0(e^{j\omega}) = 0, \quad \omega \in \Omega, \quad (34)$$

$$H_1(e^{j\omega}) = 0, \quad \omega \in \bar{\Omega}. \quad (35)$$

APPENDIX III

PERFECT RECONSTRUCTION LINEAR-PHASE FILTER BANKS

In the following, we define the class \mathcal{P}_N of perfect reconstruction linear-phase analysis filters used in Example 4, Section II-C. Two-channel filter banks whose analysis filters are both linear-phase and FIR were introduced by Nguyen and Vaidyanathan [32]. These authors considered several classes of such filters for which the associated synthesis filter bank is FIR as well. Our presentation here is very brief and is intended for completeness. The reader is referred to [32] and [5, Chapter 7] for details.

Consider the two-channel analysis/synthesis filter bank shown in Fig. 2 and assume that D is zero. Recall that the analysis filters $H_0(z)$ and $H_1(z)$ can be compactly represented by the transfer vector $\mathbf{h}(z) \triangleq [H_0(z) H_1(z)]^T$ and that $\mathbf{h}(z)$ can be factored as $\mathbf{h}(z) = \mathbf{E}(z^M)\mathbf{e}(z)$. In this factorization, $\mathbf{e}(z) \triangleq [1 z^{-1}]^T$ and $\mathbf{E}(z)$ is a type-1 polyphase matrix. The class \mathcal{P}_N of two-channel analysis filter banks is defined as those filter banks for which the following conditions are satisfied:

1. The filters $H_0(z)$ and $H_1(z)$ are of length $N \triangleq 2(K + 1)$, where $K \in \mathbb{Z}^+$ is fixed. In other words, $\mathbf{E}(z)$ is FIR of order K .
2. The matrix $\mathbf{E}(z)$ has the factorization

$$\mathbf{E}(z) = \mathbf{A}_K \mathbf{D}(z) \mathbf{A}_{K-1} \mathbf{D}(z) \dots \mathbf{D}(z) \mathbf{A}_0 \quad (36)$$

where

$$\mathbf{D}(z) \triangleq \begin{bmatrix} 1 & 0 \\ 0 & z^{-1} \end{bmatrix} \quad (37)$$

and

$$\mathbf{A}_i \triangleq \begin{bmatrix} 1 & \theta_i \\ \theta_i & 1 \end{bmatrix} \quad 0 \leq i \leq K - 1, \quad (38)$$

$$\mathbf{A}_i \triangleq \begin{bmatrix} 1 & 1 \\ 1 & -1 \end{bmatrix} \quad i = K.$$

One can verify that the above conditions result in analysis filter banks for which the impulse response of one filter is symmetric while the impulse response of the other is anti-symmetric. Thus, $H_0(z)$ and $H_1(z)$ will have linear phase. Furthermore, $|\angle H_0(e^{j\omega}) - \angle H_1(e^{j\omega})| = \frac{\pi}{2}$. The filters in \mathcal{P}_N allow perfect reconstruction with an overall delay of $K + 1$ samples. Perfect reconstruction is achieved by FIR synthesis filters which are obtained by first constructing the adjoint polyphase matrix

$$\mathbf{R}(z) = \mathbf{A}_0^T \mathbf{C}(z) \mathbf{A}_1^T \mathbf{C}(z) \dots \mathbf{C}(z) \mathbf{A}_K^T \quad (39)$$

where

$$\mathbf{C}(z) = \begin{bmatrix} z^{-1} & 0 \\ 0 & 1 \end{bmatrix}. \quad (40)$$

The synthesis filters $F_0(z)$ and $F_1(z)$ are then calculated from

$$\begin{bmatrix} f_0(z) & f_1(z) \end{bmatrix} = \mathbf{e}^T(z) \mathbf{R}(z^M). \quad (41)$$

The filter banks in the class \mathcal{P}_N are parameterized by the K free parameters θ_0 to θ_{K-1} . These parameters may be optimized such that certain frequency response requirements are satisfied or at least approximated. The analysis filters introduced in Example 4, Section II-C, were chosen to be in the class \mathcal{P}_1 . The filters in this class are parameterized by only one parameter θ_0 . For the analysis filters introduced in Example 4, this parameter was set to 78.04. This particular value was obtained by minimizing the objective function

$$\begin{aligned} \gamma &= \int_0^{\omega_{pass}} (1 - |H_0(e^{j\omega})|)^2 d\omega + \int_{\omega_{stop}}^{\pi} |H_0(e^{j\omega})|^2 d\omega \\ &+ \int_{\omega_{stop}}^{\pi} (1 - |H_1(e^{j\omega})|)^2 d\omega + \int_0^{\omega_{pass}} |H_1(e^{j\omega})|^2 d\omega \end{aligned} \quad (42)$$

with $\omega_{pass} = 0.45\pi$ and $\omega_{stop} = 0.55\pi$. This objective function reflects the mean-square deviation of the frequency responses of the filters $H_0(z)$ and $H_1(z)$ from ideal low-pass and high-pass responses, respectively⁷.

⁷Making $H_0(z)$ low-pass and $H_1(z)$ high-pass is a traditional design in filter bank literature. Whether this design has any particular merit for sensor filter applications is not known.

REFERENCES

- [1] I. F. Akyildiz, W. Su, Y. Sankarasubramaniam, and E. Cayirci, "A survey on sensor networks," *IEEE Communications Magazine*, vol. 40, no. 8, pp. 102–114, August 2002.
- [2] C. Y. Chong and S. P. Kumar, "Sensor networks: Evolution, oportunities, and challenges," *Proceedings of the IEEE*, vol. 91, no. 8, pp. 1247, August 2003.
- [3] A. V. Oppenheim and R. W. Schaffer, *Discrete-Time Signal Processing*, Prentice Hall, New Jersey, 1989.
- [4] H. Meyr, M. Moeneclaey, and S. A. Fechtel, *Digital Communication Receivers, Synchronization, Channel estimation, and Signal Processing*, Wiley Interscience, New York, NY, 1998.
- [5] P. P. Vaidyanathan, *Multirate Sytems and Filter Banks*, Prentice-Hall, Upper Saddle River, NJ, 1993.
- [6] N. J. Fliege, *Multirate Digital Signal Processing*, John Wiley, Chichester, 1994.
- [7] S. Mallat, *A Wavelet Tour of Signal Processing*, Academic Press, San Diego, CA, 2nd edition, 1999.
- [8] O. Jahromi and P. Aarabi, "Time delay estimation and signal reconstruction in multirate microphone arrays," in *Proceedings of Intl. Conf. Acoustics, Speech and Signal Processing (ICASSP)*, Hong Kong, April 2003, vol. VI, pp. 113–116.
- [9] M.S. Brandstein and H. Silverman, "A robust method for speech signal time-delay estimation in reverberant rooms," in *Proceedings of the IEEE Conference on Acoustics, Speech, and Signal Processing*, May 1996.
- [10] P. Aarabi and S. Zaky, "Robust sound localization using multi-source audiovisual information fusion," *Information Fusion*, vol. 3:2, pp. 209–223, Sept. 2001.
- [11] C. H. Knapp and G. Carter, "The generalized correlation method for estimation of time delay," *IEEE Transactions on Acoustics, Speech and Signal Processing*, vol. ASSP-24, pp. 320–327, Aug. 1976.
- [12] P. Aarabi and S. Mavandadi, "Multi-source time delays of arrival estimation using conditional time-frequency histograms," *International Journal of Information Fusion*, vol. 4, no. 2, pp. 111–122, June 2003.
- [13] P. Aarabi, *The Integration and Localization of Distributed Sensor Arrays*, Ph.D. thesis, Stanford University, May 2001.
- [14] P. Aarabi, "The fusion of distributed microphone arrays for sound localization," *EURASIP Journal of Applied Signal Processing (Special Issue on Sensor Networks)*, vol. 2003, no. 4, pp. 338–347, March 2003.
- [15] S. M. Kay, *Modern Spectrum Estimation: Theory and Applications*, Prentice Hall, Upper Saddle River, NJ, 1988.
- [16] M. H. Hayes, *Statistical Signal Processing and Modeling*, Wiley, New York, NY, 1996.
- [17] O. S. Jahromi, B. A. Francis, and R. H. Kwong, "Spectral estimation using multirate measurements," *IEEE Transactions on Signal Processing*, vol. 52, no. 7, July 2004, to appear.
- [18] T. W. Parks and J. H. McClellan, "Chebyshev approximation for nonrecursive digital filters with linear phase," *IEEE Transactions on Circuit Theory*, vol. 19, pp. 189–194, 1972.
- [19] T. W. Parks and J. H. McClellan, "A program for the design of linear phase finite impulse response digital filters," *IEEE Transactions on Audio and Electroacoustics*, vol. 20, pp. 195–199, 1972.
- [20] A. Antoniou, *Digital Filters: Analysis, Design and Applications*, McGraw-Hill, 2nd edition, 1993.
- [21] J. Lam, "Model reduction of delay systems using Padé approximation," *International Journal of Control*, vol. 57, no. 2, pp. 377–391, 1993.
- [22] M. G. Yoon and B. H. Lee, "A new approximation method for time-delay systems," *IEEE Transactions on Automatic Control*, vol. 42, no. 7, pp. 1008–1012, July 1997.

- [23] L. D. Philipp, A. Mahmood, and B. L. Philipp, "An improved refinable rational approximation to the ideal time delay," *IEEE Transactions on Circuits and Systems-I: Fundamental Theory and Applications*, vol. 46, no. 5, pp. 637–640, May 1999.
- [24] R. G. Shenoy, "Formulation of multirate filter design as an approximation problem," *Proceedings of IEEE International Symposium on Circuits and Systems (ISCAS '94)*, vol. 2, pp. 173–176, May 1994.
- [25] R. G. Shenoy, D. Burnside, and T. W. Parks, "Linear periodic systems and multirate filter design," *IEEE Transactions on Signal Processing*, vol. 42, no. 9, pp. 2242–2256, September 1994.
- [26] T. Chen and B. A. Francis, "Design of multirate filter banks by \mathcal{H}_∞ optimization," *IEEE Transactions on Signal Processing*, vol. 43, no. 12, pp. 2822–2830, December 1995.
- [27] M. Li and C. W. Kok, "Linear phase filter bank design using LMI-based \mathcal{H}_∞ optimization," *IEEE Transactions on Circuits and Systems-II: Analog and Digital Signal Processing*, vol. 50, no. 3, pp. 143–150, March 2003.
- [28] B. A. Francis, *A Course in \mathcal{H}_∞ control theory*, vol. 88 of *Lecture Notes in Control and Information Sciences*, Springer-Verlag, Berlin, 1987.
- [29] M. Green and D. J. N. Limebeer, *Linear Robust Control*, Printice-Hall, Englewood Clifes, NJ, 1995.
- [30] T. Chen and B. A. Francis, *Optimal Sampled Data Control Systems*, Springer-Verlag, London, 1995.
- [31] V. Sathe and P. P. Vaidyanathan, "Effect of multirate systems on the statistical properties of random signals," *IEEE Transactions on Acoustics, Speech and Signal Processing*, vol. 41, no. 1, pp. 131–146, January 1993.
- [32] T. Q. Nguyen and P. P. Vaidyanathan, "Two-channel perfect-reconstruction FIR QMF structures which yield linear-phase analysis and synthesis filters," *IEEE Transactions on Signal Processing*, vol. 37, no. 5, May 1989.